

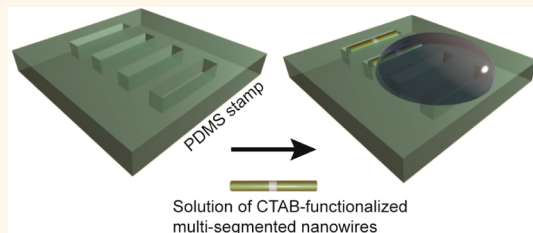
# Capillary Force-Driven, Large-Area Alignment of Multi-segmented Nanowires

Xiaozhu Zhou,<sup>†,§</sup> Yu Zhou,<sup>‡,§</sup> Jessie C. Ku,<sup>‡</sup> Chuan Zhang,<sup>†</sup> and Chad A. Mirkin<sup>†,‡,\*</sup>

<sup>†</sup>Department of Chemistry and International Institute for Nanotechnology, Northwestern University, 2145 Sheridan Road, Evanston, Illinois 60208, United States

<sup>‡</sup>Department of Materials Science and Engineering, Northwestern University, 2220 Campus Drive, Evanston, Illinois 60208, United States. <sup>§</sup>X.Z. and Y.Z. contributed equally.

**ABSTRACT** We report the large-area alignment of multi-segmented nanowires in nanoscale trenches facilitated by capillary forces. Electrochemically synthesized nanowires between 120 and 250 nm in length are aligned and then etched selectively to remove one segment, resulting in arrays of nanowires with precisely controlled gaps varying between 2 and 30 nm. Crucial to this alignment process is the dispersibility of the nanowires in solution which is achieved by chemically modifying them with hexadecyltrimethylammonium bromide. We found that, even without the formation of an ordered crystalline phase at the droplet edges, the nanowires can be aligned in high yield. To illustrate the versatility of this approach as a nanofabrication technique, the aligned nanowires were used for the fabrication of arrays of gapped graphene nanoribbons and SERS substrates.



**KEYWORDS:** multi-segmented nanowire · capillary force · alignment · on-wire lithography · graphene nanoribbon · SERS

There has been an increasing interest in the synthesis and application of anisotropic nanostructures due to their rich plasmonic, optoelectronic, and catalytic properties.<sup>1–4</sup> Among them, on-wire lithography (OWL)-generated gapped nanowires<sup>5–11</sup> have received widespread interest and show promise in various fields, including plasmonics, surface-enhanced Raman spectroscopy (SERS), nanoencoding, and molecular electronics.<sup>12–15</sup> Because of the fine control OWL provides over metal segment length and gap size, the technique has been used for the systematic investigation of the structure–function relationships for segmented wires of a wide variety of compositions and lengths, opening avenues to new nanowire applications.<sup>12</sup> For example, the localized surface plasmon resonance wavelength can be tailored deliberately by simply changing the gap size in 35 nm diameter dimer structures consisting of two 70 nm long gold segments.<sup>7</sup> Such OWL nanostructures have been used to understand the origins of hotspots in SERS and create novel taggants, known as SERS nanosheets.<sup>16</sup> In addition, we have recently demonstrated that these OWL-generated nanowires can be used as etch masks to make gapped graphene nanoribbons (GNRs).<sup>17</sup> However, in order to realize the full potential

of OWL-generated nanostructures, it is imperative that methods for assembling them over large areas with control over position, orientation, and density be developed. Arrays of OWL nanostructures are of particular interest for SERS applications since, in principle, more uniform Raman signals can be obtained from ordered arrays of gapped nanowires as opposed to randomly oriented and spaced structures. Furthermore, it may be possible to use aligned OWL nanostructures as etch masks, providing methods for translating large patterns consisting of gapped nanowires into underlying substrates. This capability would be potentially useful for a broad range of applications, spanning electronics,<sup>18,19</sup> plasmonics<sup>20</sup> and metamaterials.<sup>21</sup>

Thus far, a few methods have been developed for preparing large arrays of multi-segmented nanowires. For example, Xu *et al.* have utilized prepatterned arrays of nanomagnets to align nanowires that contain magnetic Ni segments.<sup>22</sup> Although a significant step forward, the disadvantages of this method are the low yield and poor control over wire number and orientation. In addition, the requirement of prefabricating arrays of nanomagnets makes this method less straightforward. Our group has developed a brush method to mechanically align multi-segmented nanowires.<sup>23</sup> However, this

\* Address correspondence to chadnano@northwestern.edu.

Received for review October 28, 2013 and accepted January 13, 2014.

Published online January 22, 2014  
10.1021/nn405627s

© 2014 American Chemical Society

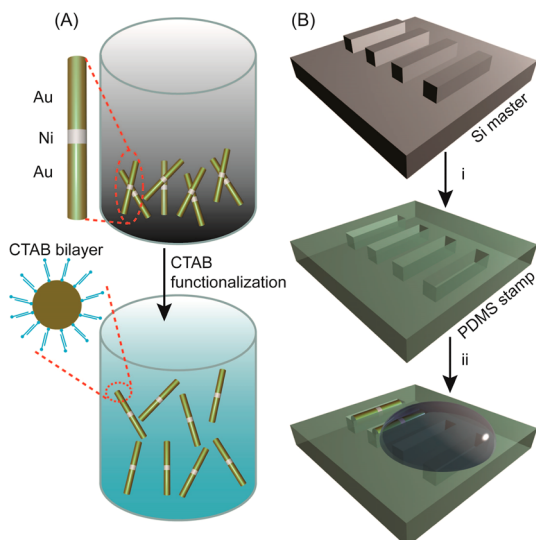


**Figure 1. Schematic illustration of the alignment of multi-segmented nanowires into trenches by capillary forces.** (A) Functionalization of nanowires with CTAB in a 0.45 mM CTAB aqueous solution. Coating of a bilayer CTAB on the surface of the nanowires prevents their aggregation and increases the stability of the suspension. (B) (i) Fabrication of PDMS stamp with negative trenches by curing elastomers on a silicon master with positive features. (ii) Alignment of nanowires into the trenches when a drop of nanowire solution moves across the trench area driven by a drying process (*via* heating).

method is only effective for micrometer long nanowires due to the large size of the brush hair (micrometer scale) and is not suitable for aligning single wires. Fluid-based methods have been reported for the alignment of nanoparticles. However, either single-particle resolution is not achievable or the method requires the preformation of a floating nanoparticle film<sup>24</sup> or the presence of fluid in the trenches.<sup>25</sup> Recently, methods that utilize capillary forces to assemble chemically synthesized spherical and rod-like gold particles in predefined trenches<sup>26–28</sup> have shown promise for assembling individual and collections of particles on prepatterned substrates. However, with these methods, challenges exist in achieving precise control over interparticle distance for multiple particles within one trench, which is a necessity for a variety of applications such as local field enhancement in SERS-active structures. Since OWL allows one to prepare nanostructures separated by multiple well-defined nanoscale gaps, a method to assemble such structures with capillary forces could provide a straightforward way of aligning dimers or multimers with precise control over interparticle distance.

Herein, we report the large-area assembly of electrochemically synthesized multi-segmented nanowires of different gap sizes, lengths, and aspect ratios with control over wire position and orientation (Figure 1). To show prototypical electronic and optical devices based on these structures, we evaluated their use as masks for the fabrication of arrays of gapped graphene

nanoribbons and as SERS substrates for the detection of small molecules.

## RESULTS AND DISCUSSION

In a typical experiment, nanowires with alternating segments of Au and Ni were synthesized electrochemically (see Methods section for details). This was followed by functionalization with hexadecyltrimethylammonium bromide (CTAB) and stabilization in a 0.45 mM CTAB aqueous solution (Figure 1A). The solution was then dropped onto a PDMS stamp with trenches that were made by molding the elastomer on a silicon master with raised features (Figure 1B and Figure S1 in the Supporting Information). During the drying process (the stamp was heated at 50 °C), the droplet edge spontaneously shrank due to solvent evaporation and moved over the trench area, and the nanowires were aligned into the trenches by nanoscale capillary forces over a 200 × 500  $\mu\text{m}^2$  area.

Electrochemically synthesized nanowires differ from many previously studied wires in that they are not capped by a surfactant. Therefore, we hypothesized that in order to reliably control the assembly of electrochemically synthesized nanowires, their surface functionality must be controlled. We selected CTAB because it has been widely used in the synthesis of gold nanoparticles as a shape-directing agent and stabilizing surfactant.<sup>29,30</sup> To functionalize nanowires with CTAB, as-synthesized nanowires were rigorously washed with a 0.45 mM CTAB aqueous solution and then dispersed in the 0.45 mM CTAB solution (detailed procedures can be found in the Methods section). Following functionalization, the nanowires exhibited a positive zeta-potential (48 mV) and were stable in solution for up to 24 h (Figure S2, Supporting Information), leading us to conclude that they were functionalized with a bilayer of CTAB.<sup>31</sup> It is important to note that if as-synthesized nanowires were used without CTAB modification, a very low yield of alignment was obtained (percentage of trenches occupied by nanowires, <5%). Even when the nanowires were functionalized with 1,4-benzenedithiol (1,4-BDT), which provides moderate stability when transferred to 0.45 mM CTAB solution (precipitation occurred within 3 h), a typical alignment yield was still less than 20%. Although we are primarily focused on the assembly of multi-segmented nanowires, this approach should be applicable to other types of nanowires, for example, Si nanowires, as long as they can be properly functionalized with surfactants to make them dispersible in solution (e.g., no precipitation for up to 24 h).

Next, we evaluated the potential of using PDMS with well-defined trenches to align multi-segmented nanowires with different compositions and lengths (Figure 2A,C–E). Through experimentation, we found that the alignment yield is very sensitive to the dimensions of the trenches. In order to optimize the alignment,

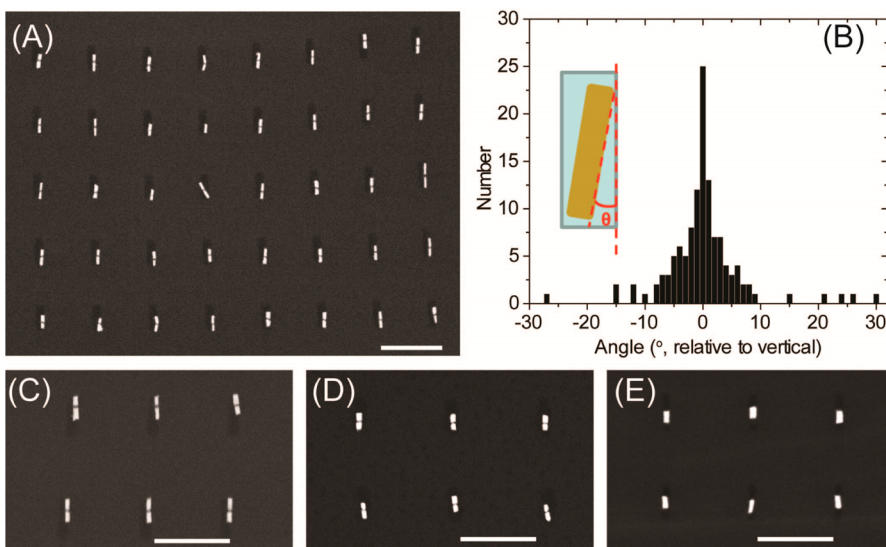


**Figure 2.** Representative SEM images and angle statistics of the aligned multi-segmented nanowires. (A) Array of aligned nanowires consisting of two Au segments separated by a short Ni segment. (B) Distribution of the orientation of aligned nanowires with a length of 250 nm. The inset schematic shows how the alignment angle  $\theta$  is measured. The width of the histogram bar is  $1^\circ$ . (C–E) Arrays of nanowires with a diameter of 35 nm and consisting of Au and Ni segment with different lengths: (C) Total length =  $252 \pm 24$  nm, Ni segment =  $29 \pm 4$  nm, aspect ratio = 7. (D) Total length =  $177 \pm 9$  nm, Ni segment =  $11 \pm 3$  nm, aspect ratio = 5. (E) Total length =  $125 \pm 8$  nm, Ni segment =  $2 \pm 0.4$  nm, aspect ratio = 3.5. Scale bars: 1  $\mu$ m.

including yield, orientation, and transfer rate, trenches of varying dimensions were systematically assessed. For 250 nm long nanowires, trenches that vary from 350 to 450 nm in length, from 70 to 120 nm in width, and from 35 to 50 nm in depth were studied. High alignment yield (>85%) was achieved when trenches of 400 nm  $\times$  80 nm  $\times$  39 nm dimensions were used (Figure 2A). If the dimensions of the trench are similar to the size of the nanowires, only very few can be trapped (yield <5%). The trenches must be larger than the nanowires (with a length of 250 nm and a diameter of 35 nm) for two reasons. First, larger trenches can provide a stronger capillary force and therefore increase the contact line pinning effect,<sup>32</sup> which is important in the control of droplet evaporation dynamics by obtaining a slow shrinking speed ( $\sim 2 \mu\text{m/s}$ ) so that nanowires have enough time to be trapped. Second, because of the disordered arrangement of the nanowires at the droplet edge (Figure 3A), a larger trench is needed to provide extra room for the nanowires to adjust orientation and fit within it. Interestingly, 95% of the nanowires were aligned by capillary immersion forces<sup>28</sup> to the corners of the trenches in the same direction as that of the moving droplet edge. As a result, a narrow angle distribution was obtained, with 92% of the nanowires aligned within  $10^\circ$  with respect to vertical (Figure 2B). In addition to the effect of trench size on alignment, we also evaluated the influence of nanowire concentration, humidity, and temperature on the process. Specifically, similar alignment yields were obtained with nanowire concentrations that varied by as much as a factor of 10 (0.1 to 1 nM), leading us to the conclusion that nanowire concentration is not a sensitive parameter in the alignment process.

This is because the nanowire concentration is always high within the densely packed zone (Figure 3A), regardless of the solution concentration. At high humidity (70% RH) or low temperatures ( $25^\circ\text{C}$ ), it is difficult to form a densely packed zone of nanowires at the droplet edge due to slow solvent evaporation. This results in a much lower alignment yield (<20%).

To test the generality of the technique, we prepared a set of gapped nanowires with an average diameter of 35 nm and lengths varying between 120 and 250 nm and studied their assembly behavior in the PDMS with well-defined trenches (Figure 2C–E). The nanowires have aspect ratios (defined as  $L/D$ , where  $L$  and  $D$  are the length and diameter of the nanowire) varying between 3.5 and 7. All of the wires could be aligned on the PDMS substrates in high yield, provided the appropriate trench architectures were used, as summarized in Table S1 (Supporting Information). Specifically, the length and width of the trench should be *ca.* 150 and 40 nm larger than those of the nanowires, respectively, in order to obtain high yield. The successful alignment of nanowires with an aspect ratio of 7, larger than previously reported value of 3,<sup>27</sup> is particularly encouraging since it opens possibilities for assembling nanowires that are exceedingly long (e.g., silicon nanowires<sup>33</sup>) and important for applications such as electronics. Different functionalization protocols may be needed owing to different surface chemistries for other types of nanowires, but conceptually the technique should be extendible to other compositions.

Remarkably, we obtained high-yield alignment of the nanowires even though a disordered phase was formed for multi-segmented nanowire aggregates at

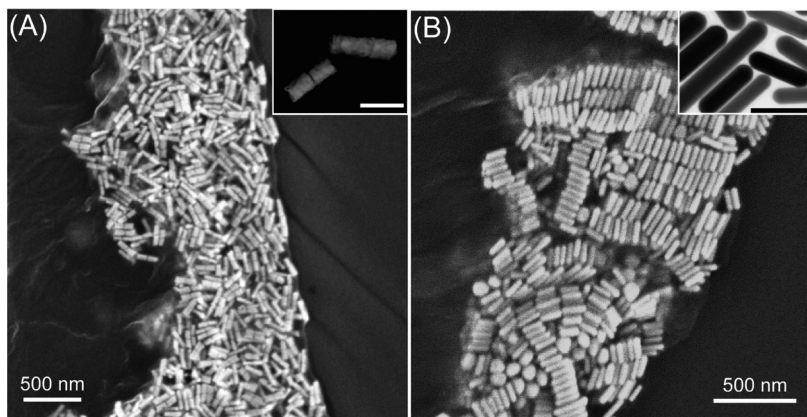


**Figure 3.** SEM image comparison of the accumulation zone of nanowires synthesized through the (A) OWL method and (B) surfactant-mediated chemical reduction method. (A) Disordered domains are formed due to rough wire surfaces (inset, TEM image) of the multi-segmented nanowires. (B) Ordered domains are formed due to accumulation of the nanorods with atomically smooth surfaces (inset, TEM image). Inset scale bars: 80 nm.

the droplet edge (Figure 3A). In a study where chemically synthesized rod-like nanoparticles with an aspect ratio of 3 were used, the formation of an ordered crystalline phase was argued to be a prerequisite for the high-yield alignment of wires.<sup>27</sup> However, in our study, the electrochemically synthesized multi-segmented nanowires have rough surfaces due to the rough pores in the AAO template<sup>34</sup> (Figure 3A, inset). As a result, it is difficult for the nanowires to pack closely and form ordered phases (Figure 3A). This is in contrast to that of many chemically synthesized nanorods that possess atomically flat surfaces, which facilitate the formation of crystalline phases (Figure 3B). In our study, we found that nanowires started to be trapped when the contact angle of the droplet is very small (*i.e.*,  $\sim 25^\circ$ , Figure S3). The assembly of spherical nanoparticles has indeed been reported at such low contact angles.<sup>35</sup>

Thus far, we have primarily discussed segmented wires, but gapped nanowires can also be prepared using a variant of the aforementioned method. For example, segmented wires consisting of alternating Au and Ni segments can be transferred to desired substrates through microcontact printing<sup>27</sup> (Figure 4A). In typical experiments, prior to the transfer, the substrate ( $\text{SiO}_2$  in this case) was spin-coated with a thin film (*ca.* 20 nm) of PMMA (495 K, Microchem) which serves as an adhesive layer to promote a high transfer yield (>95%) and secures the positions of the nanowires to prevent them from migrating during subsequent processing steps. The role of the PMMA is analogous to that of the silica backing layer in conventional OWL.<sup>5</sup> The nanowires were then transferred to the target substrate by heating it to 135 °C and applying pressure to the PDMS stamp against the substrate for 1 min (Figure 4A,i), followed by air cooling to room temperature and removal of pressure (Figure 4A,ii). After the transfer, Ni was etched in a HCl aqueous solution and gapped nanowire arrays were created (Figure 4B).

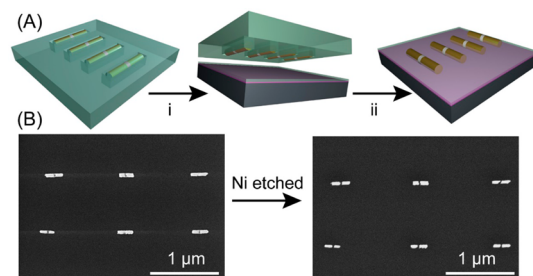


**Figure 4.** Transfer of multi-segmented nanowire arrays to a target substrate (*e.g.*, graphene) by microcontact printing. (A) (i) Positioning nanowire arrays on top of graphene with a homemade micromanipulator. (ii) Nanowires are transferred by applying pressure on the stamp against the target substrate at 135 °C. (B) SEM images of the transferred nanowires on a single layer of graphene, before and after Ni etching. Nanowires with 29 nm Ni segment (Figure 2C) were used, and 29 nm gaps were thus created. The registry of Au segments is maintained.

Finally, we explored two applications for the transferred nanowires. Following the strategy of our previous work,<sup>17</sup> an array of gapped GNRs was fabricated using the aligned gapped nanowires as etch masks. As described above, the nanowire arrays were first transferred to a PMMA-coated graphene sample (Figure S4), followed by Ni etching and gap formation. Thereafter, the graphene sample was etched with reactive ion etching and then sonicated in acetone to remove the remaining PMMA and reveal the gapped GNRs (Figure 5A). The gap size in these nanoribbons is  $\sim 25$  nm, matching the length of the Ni segment in the nanowires. The ribbon array was further characterized by Raman mapping (Figure S5). This aligned array of GNRs affords interesting graphene structures that may prove useful for electronics<sup>18,19</sup> and plasmonics<sup>20,21,36</sup> considering that the gap size, ribbon length, and ribbon-to-ribbon distance are highly adjustable.

Another important application of these nanowires is to utilize them as SERS substrates. As proof-of-concept, nanowires consisting of two 60 nm gold segments and

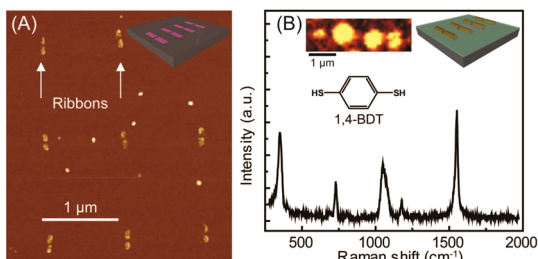


**Figure 5.** Fabrication of gapped graphene nanoribbons and SERS substrate. (A) Aligned graphene nanoribbons generated by using the gapped nanowires from Figure 4B as etch masks. Nanoribbons 200 nm long with a gap of  $\sim$ 25 nm were fabricated. (B) SERS measurement of 1,4-BDT from aligned gapped nanowires. A row of hot spots is shown in the top-left inset; a.u., arbitrary units.

a 2 nm Ni segment were designed and synthesized. Alignment of the nanowires on a PMMA-coated silicon substrate and etching of the Ni segments yielded arrays of Au dimer structures with a plasmon resonance centered at 785 nm, matching that of the laser wavelength used in the Raman measurement. The gold nanostructures were then functionalized with 1,4-BDT by incubating the substrate in an ethanol solution ( $\sim$ 1 mM) for 12 h. These nanostructures have been previously shown to be local amplifiers for surface-enhanced Raman scattering with enhancement factors of  $7 \times 10^8$ .<sup>37</sup> Raman mapping clearly reveals strong SERS signals (e.g., C–C stretch mode at  $\sim$ 1561 cm<sup>-1</sup>) from 1,4-BDT when the laser is scanned

across the array (Figure 5B). It is worth mentioning that the density of nanowires can be adjusted by simply changing the trench design (Figure S6). Thus, the aligned gapped nanowires provide a route to new SERS substrates with uniform distributions of hot spots that can be used for a variety of chemical and biological sensor applications.<sup>38</sup>

## CONCLUSIONS

In summary, we have developed a large-area alignment strategy for electrochemically synthesized multi-segmented nanowires with control over position, orientation, and density by using a nanoscale capillary force-mediated assembly method. Importantly, we are able to align nanowires with different gap sizes, lengths, and aspect ratios. The high-yield alignment of nanowires with an aspect ratio as large as 7 is particularly encouraging for many applications that require high aspect ratio nanostructures. As one of the critical conditions for the alignment, the excellent wire dispersibility by CTAB functionalization is promising for many other types of nanostructures that are synthesized without surfactant modification, for example, Si nanowires<sup>33</sup> and ZnO nanorods.<sup>39</sup> The proof-of-concept experiments demonstrating the fabrication of arrays of graphene nanoribbons and SERS substrates make the technique particularly attractive to researchers who require these kind of structures for a variety of electronic, spectroscopic, and plasmonic applications.<sup>36,40</sup>

## METHODS

**Synthesis of Multi-segmented Metal Nanowires and Functionalization with Hexadecyltrimethylammonium Bromide.** Multi-segmented nanowires consisting of Au–Ni–Au were electrochemically synthesized in anodized aluminum oxide (AAO) membranes from Synkera Technologies, Inc. having a manufacturer-specified pore diameter of 35 nm. The general electrochemical deposition process has been described in the literature.<sup>6,7</sup> Specifically, nanowires with different lengths (110 nm Au/29 nm Ni/110 nm Au: nanowire 1; 80 nm Au/11 nm Ni/80 nm Au: nanowire 2; 60 nm Au/2 nm Ni/60 nm Au: nanowire 3) were synthesized and used for the alignment process. The synthesized nanowires were functionalized with hexadecyltrimethylammonium bromide in a 0.45 mM CTAB aqueous solution. Repeated centrifugation, resuspension, and incubation of the nanowires to new CTAB solutions (up to 8 iterations) will ensure successful functionalization of CTAB which is evidenced by the fact that the nanowires remain in a pseudoliquid state when centrifuged and can be easily dispersed when adding new CTAB solution (without the need for sonication).

**Silicon Master and PDMS Stamp Fabrication.** A silicon master with positive linelet arrays was made by e-beam lithography using negative-tone resist hydrogen silsesquioxane (HSQ). A PDMS stamp (10:1 elastomer to curing agent using SYLGARD 184 SILICONE ELASTOMER KIT) with negative trenches was made from the master by curing the elastomer precursor at 80 °C for 3 h. The specific dimensions of the trenches and nanowires used are summarized in Table S1.

**Alignment of Nanowires into Elastomer Trenches.** A droplet (5  $\mu$ L) of nanowire solution (0.45 mM CTAB aqueous solution) was dropped on the PDMS stamp trench region under an optical microscope. The PDMS stamp was then heated on a hot plate at

50 °C, allowing the droplet to dry while the edge of the drop moves simultaneously across the trench region. The nanowires are aligned into the trenches due to capillary forces.

### Transfer of Aligned Nanowires to Graphene and Silicon Substrates.

The aligned nanowires were transferred to either a PMMA-coated graphene substrate for the fabrication of arrays of graphene nanoribbons or a PMMA-coated silicon substrate in the case of SERS-active substrate. PMMA adhesion layer and heating at 135 °C facilitate the transfer of nanowires. Arrays of graphene nanoribbons were fabricated according to a previous report.<sup>17</sup> Raman mapping for SERS was carried out on a Witec instrument using 785 nm laser with a power of  $\sim$ 1 mW.

**Conflict of Interest:** The authors declare no competing financial interest.

**Acknowledgment.** This material is based upon work supported by the AFOSR under Award Nos. FA9550-09-1-0294 and FA9550-12-1-0280, and the AOARD under Award No. FA2386-13-1-4124. This material is based upon work supported by the Office of the Asst. Secretary of Defense for Research and Engineering, DoD/NSSEFF Program/Naval Postgraduate School under Award Nos. N00244-09-1-0012 and N00244-09-1-0071. This material is based upon work supported by the Department of the Navy, Office of Naval Research under Award No. N00014-11-1-0729. J.C.K. acknowledges the Department of Defense for a National Defense Science and Engineering Graduate Fellowship. Y.Z. acknowledges a Northwestern University Ryan Fellowship.

**Supporting Information Available:** Additional AFM image, SEM images, optical graph, UV–vis spectra, and Raman mapping. This material is available free of charge via the Internet at <http://pubs.acs.org>.

## REFERENCES AND NOTES

- Burda, C.; Chen, X.; Narayanan, R.; El-Sayed, M. A. Chemistry and Properties of Nanocrystals of Different Shapes. *Chem. Rev.* **2005**, *105*, 1025–1102.
- Jones, M. R.; Osberg, K. D.; Macfarlane, R. J.; Langille, M. R.; Mirkin, C. A. Templated Techniques for the Synthesis and Assembly of Plasmonic Nanostructures. *Chem. Rev.* **2011**, *111*, 3736–3827.
- Wall, B. D.; Diegelmann, S. R.; Zhang, S.; Dawidczyk, T. J.; Wilson, W. L.; Katz, H. E.; Mao, H.-Q.; Tovar, J. D. Aligned Macroscopic Domains of Optoelectronic Nanostructures Prepared via Shear-Flow Assembly of Peptide Hydrogels. *Adv. Mater.* **2011**, *23*, 5009–5014.
- Komanicky, V.; Iddir, H.; Chang, K. C.; Menzel, A.; Karapetrov, G.; Hennessy, D.; Zapol, P.; You, H. Shape-Dependent Activity of Platinum Array Catalyst. *J. Am. Chem. Soc.* **2009**, *131*, 5732–5733.
- Qin, L.; Park, S.; Huang, L.; Mirkin, C. A. On-Wire Lithography. *Science* **2005**, *309*, 113–115.
- Banholzer, M. J.; Qin, L.; Millstone, J. E.; Osberg, K. D.; Mirkin, C. A. On-Wire Lithography: Synthesis, Encoding and Biological Applications. *Nat. Protoc.* **2009**, *4*, 838–848.
- Osberg, K. D.; Schmucker, A. L.; Senesi, A. J.; Mirkin, C. A. One-Dimensional Nanorod Arrays: Independent Control of Composition, Length, and Interparticle Spacing with Nanometer Precision. *Nano Lett.* **2011**, *11*, 820–824.
- Rivera, T. P.; Lecarme, O.; Hartmann, J.; Inglebert, R. L.; Peyrade, D. Spectroscopic Studies of Plasmonic Interactions in Colloidal Dimers Fabricated by Convective-Capillary Force Assembly. *Microelectron. Eng.* **2009**, *86*, 1089–1092.
- Jiang, L.; Sun, Y.; Huo, F.; Zhang, H.; Qin, L.; Li, S.; Chen, X. Free-Standing One-Dimensional Plasmonic Nanostructures. *Nanoscale* **2012**, *4*, 66–75.
- Liusman, C.; Li, S.; Chen, X.; Wei, W.; Zhang, H.; Schatz, G. C.; Boey, F.; Mirkin, C. A. Free-Standing Bimetallic Nanorings and Nanoring Arrays Made by On-Wire Lithography. *ACS Nano* **2010**, *4*, 7676–7682.
- Liusman, C.; Li, H.; Lu, G.; Wu, J.; Boey, F.; Li, S.; Zhang, H. Surface-Enhanced Raman Scattering of Ag–Au Nanodisk Heterodimers. *J. Phys. Chem. C* **2012**, *116*, 10390–10395.
- Qin, L.; Zou, S.; Xue, C.; Atkinson, A.; Schatz, G. C.; Mirkin, C. A. Designing, Fabricating, and Imaging Raman Hot Spots. *Proc. Natl. Acad. Sci. U.S.A.* **2006**, *103*, 13300–13303.
- Wei, W.; Li, S.; Millstone, J. E.; Banholzer, M. J.; Chen, X.; Xu, X.; Schatz, G. C.; Mirkin, C. A. Surprisingly Long-Range Surface-Enhanced Raman Scattering (SERS) on Au–Ni Multisegmented Nanowires. *Angew. Chem., Int. Ed.* **2009**, *48*, 4210–4212.
- Qin, L.; Banholzer, M. J.; Millstone, J. E.; Mirkin, C. A. Nanodisk Codes. *Nano Lett.* **2007**, *7*, 3849–3853.
- Chen, X.; Yeganeh, S.; Qin, L.; Li, S.; Xue, C.; Braunschweig, A. B.; Schatz, G. C.; Ratner, M. A.; Mirkin, C. A. Chemical Fabrication of Heterometallic Nanogaps for Molecular Transport Junctions. *Nano Lett.* **2009**, *9*, 3974–3979.
- Osberg, K. D.; Rycenga, M.; Bourret, G. R.; Brown, K. A.; Mirkin, C. A. Dispersible Surface-Enhanced Raman Scattering Nanosheets. *Adv. Mater.* **2012**, *24*, 6065–6070.
- Zhou, X.; Shade, C. M.; Schmucker, A. L.; Brown, K. A.; He, S.; Boey, F.; Ma, J.; Zhang, H.; Mirkin, C. A. OWL-Based Nano-masks for Preparing Graphene Ribbons with Sub-10 nm Gaps. *Nano Lett.* **2012**, *12*, 4734–4737.
- Son, J. G.; Son, M.; Moon, K. J.; Lee, B. H.; Myoung, J. M.; Strano, M. S.; Ham, M. H.; Ross, C. A. Sub-10 nm Graphene Nanoribbon Array Field-Effect Transistors Fabricated by Block Copolymer Lithography. *Adv. Mater.* **2013**, *25*, 4723–4728.
- Jiao, L.; Zhang, L.; Ding, L.; Liu, J.; Dai, H. Aligned Graphene Nanoribbons and Crossbars from Unzipped Carbon Nanotubes. *Nano Res.* **2010**, *3*, 387–394.
- Freitag, M.; Low, T.; Zhu, W.; Yan, H.; Xia, F.; Avouris, P. Photocurrent in Graphene Harnessed by Tunable Intrinsic Plasmons. *Nat. Commun.* **2013**, *4*, 1951.
- Ju, L.; Geng, B.; Horng, J.; Girit, C.; Martin, M.; Hao, Z.; Bechtel, H. A.; Liang, X.; Zettl, A.; Shen, Y. R. Graphene Plasmonics for Tunable Terahertz Metamaterials. *Nat. Nanotechnol.* **2011**, *6*, 630–634.
- Xu, X.; Kim, K.; Li, H.; Fan, D. L. Ordered Arrays of Raman Nanosensors for Ultrasensitive and Location Predictable Biochemical Detection. *Adv. Mater.* **2012**, *24*, 5457–5463.
- Lim, J. K.; Lee, B. Y.; Pedano, M. L.; Senesi, A. J.; Jang, J. W.; Shim, W.; Hong, S.; Mirkin, C. A. Alignment Strategies for the Assembly of Nanowires with Submicron Diameters. *Small* **2010**, *6*, 1736–1740.
- Huang, J.; Kim, F.; Tao, A. R.; Connor, S.; Yang, P. Spontaneous Formation of Nanoparticle Stripe Patterns through Dewetting. *Nat. Mater.* **2005**, *4*, 896–900.
- Krishnan, M.; Mojarrad, N.; Kukura, P.; Sandoghdar, V. Geometry-Induced Electrostatic Trapping of Nanometric Objects in a Fluid. *Nature* **2010**, *467*, 692–695.
- Kraus, T.; Malaquin, L.; Schmid, H.; Riess, W.; Spencer, N. D.; Wolf, H. Nanoparticle Printing with Single-Particle Resolution. *Nat. Nanotechnol.* **2007**, *2*, 570–576.
- Kuemin, C.; Nowack, L.; Bozano, L.; Spencer, N. D.; Wolf, H. Oriented Assembly of Gold Nanorods on the Single-Particle Level. *Adv. Funct. Mater.* **2012**, *22*, 702–708.
- Gordon, M. J.; Peyrade, D. Separation of Colloidal Nanoparticles Using Capillary Immersion Forces. *Appl. Phys. Lett.* **2006**, *89*, 053112–3.
- Millstone, J. E.; Park, S.; Shuford, K. L.; Qin, L.; Schatz, G. C.; Mirkin, C. A. Observation of a Quadrupole Plasmon Mode for a Colloidal Solution of Gold Nanoprism. *J. Am. Chem. Soc.* **2005**, *127*, 5312–5313.
- Nikoobakht, B.; El-Sayed, M. A. Preparation and Growth Mechanism of Gold Nanorods (NRs) Using Seed-Mediated Growth Method. *Chem. Mater.* **2003**, *15*, 1957–1962.
- Murphy, C. J.; Sau, T. K.; Gole, A. M.; Orendorff, C. J.; Gao, J.; Gou, L.; Hunyadi, S. E.; Li, T. Anisotropic Metal Nanoparticles: Synthesis, Assembly, and Optical Applications. *J. Phys. Chem. B* **2005**, *109*, 13857–13870.
- Ondarçuhu, T.; Piednoir, A. Pinning of a Contact Line on Nanometric Steps during the Dewetting of a Terraced Substrate. *Nano Lett.* **2005**, *5*, 1744–1750.
- Freer, E. M.; Grachev, O.; Duan, X.; Martin, S.; Stumbo, D. P. High-Yield Self-Limiting Single-Nanowire Assembly with Dielectrophoresis. *Nat. Nanotechnol.* **2010**, *5*, 525–530.
- Martinson, A. B. F.; Elam, J. W.; Hupp, J. T.; Pellin, M. J. ZnO Nanotube Based Dye-Sensitized Solar Cells. *Nano Lett.* **2007**, *7*, 2183–2187.
- Malaquin, L.; Kraus, T.; Schmid, H.; Delamarche, E.; Wolf, H. Controlled Particle Placement through Convective and Capillary Assembly. *Langmuir* **2007**, *23*, 11513–11521.
- Yan, H.; Low, T.; Zhu, W.; Wu, Y.; Freitag, M.; Li, X.; Guinea, F.; Avouris, P.; Xia, F. Damping Pathways of Mid-infrared Plasmons in Graphene Nanostructures. *Nat. Photonics* **2013**, *7*, 394–399.
- Osberg, K. D.; Rycenga, M.; Harris, N.; Schmucker, A. L.; Langille, M. R.; Schatz, G. C.; Mirkin, C. A. Dispersible Gold Nanorod Dimers with Sub-5 nm Gaps as Local Amplifiers for Surface-Enhanced Raman Scattering. *Nano Lett.* **2012**, *12*, 3828–3832.
- Stiles, P. L.; Dieringer, J. A.; Shah, N. C.; Van Duyne, R. P. Surface-Enhanced Raman Spectroscopy. *Annu. Rev. Anal. Chem.* **2008**, *1*, 601–626.
- Sun, Y.; Fuge, G. M.; Ashfold, M. N. R. Growth of Aligned ZnO Nanorod Arrays by Catalyst-Free Pulsed Laser Deposition Methods. *Chem. Phys. Lett.* **2004**, *396*, 21–26.
- Chang, W.-S.; Ha, J. W.; Slaughter, L. S.; Link, S. Plasmonic Nanorod Absorbers as Orientation Sensors. *Proc. Natl. Acad. Sci. U.S.A.* **2010**, *107*, 2781–2786.